Advances in Applied Mathematics and Mechanics
Adv. Appl. Math. Mech., Vol. **16**, No. 1, pp. 253-278

DOI: 10.4208/aamm.OA-2021-0186
February 2024

Free Vibration of Stiffened Plate with Cracked Stiffeners

Jian Xue[1,2], Lihua Chen[1,*], Yue Sun[3] and Wei Zhang[1]

[1] *Faculty of Materials and Manufacturing, Beijing University of Technology, Beijing 100124, China*
[2] *Department of Mechanics, School of Science, Harbin Institute of Technology, Shenzhen, Guangdong 518055, China*
[3] *Institute of Textiles and Clothing, The Hong Kong Polytechnic University, Hong Kong, China*

Received 25 May 2021; Accepted (in revised version) 16 December 2022

Abstract. In this paper, a new cracked stiffener model for the stiffener with a part-through and open crack is proposed, considering the compatibility condition of displacements between the plate and the stiffener. Based on the first-order shear deformation theory, the free vibration of stiffened isotropic plates with cracked stiffeners are investigated for the first time. The description of the crack parameters is based on the continuous equivalent bending stiffness and equivalent depth of the cracked beam, and it takes into consideration of shear deformation, bending-extensional coupling vibration, and eccentricity between the stiffeners and the plate. The stiffened plates with single or multiple cracked stiffeners are formulated and discussed. The Ritz method with the modified characteristic functions is applied to demonstrate the effects of crack parameters (crack depth and location) coupling with the position and number of the cracked stiffeners on the vibration frequencies and modes of the stiffened plate. The validity and accuracy of the present solutions are verified through convergence studies and compared with the finite element results.

AMS subject classifications: 65M10, 78A48

Key words: Free vibration, stiffened plate, cracked stiffener model, crack, Ritz method.

1 Introduction

As an essential class of engineering structures, the stiffened plate is extensively used in various fields such as aircraft and ship structures. The vibration of stiffened plates has been investigated through various analytical and numerical techniques. As Mukherjee a-

*Corresponding author.
Email: chenlihua@bjut.edu.cn (L. Chen)

nd Mukhopadhyay [1] summarized in their review papers, two types of models were adopted for stiffened plates in the early literature: one is the orthotropic model in which the plate was treated as an equivalent orthotropic plate with the consideration of contribution of the stiffeners; the other is the grillage approximation model in which the stiffeners ware considered as a grid attaching to the plate. Recently, a "discrete" modeling method [2] was proposed to separately create the models of the plate and its stiffening beam. Afterwards, a complete model is formed to incorporate the displacements of the plate and the stiffener through the condition for compatibility of displacement. Many previous efforts have been devoted to the static and dynamic analysis of stiffened plates based on various methods such as the Ritz method [3–5], the finite element method [6–10], the dynamic stiffness method [11–14], the differential quadrature method [15] and the meshless method [16, 17].

When a stiffened structure is ceaselessly subjected to large irregular load or cyclic load, a fatigue crack maybe thus initiate. The existence of cracks would significantly change the dynamic characteristics of the plate [18–21]. It will be a serious issue when a crack occurs in a stiffened plate since the crack reduces the stiffness of the structure and eventually leads to an unexpected failure of the structure. Many previous studies have investigated the influence of the crack on the vibration and stability of stiffened plates. Li et al. [22–24] established an extended layerwise method and extended finite element method (XFEM) for the laminated composite plates and stiffened plates. The proposed method considered the multiple delaminations and transverse crack simultaneously. Dang and Kapania [25] analyzed the buckling of a cracked-orthogonally stiffened panel via the Ritz method in which the locally distributed trigonometric series as the admissible function of displacement was adopted. Milazzo and Oliveri [26] presented a PB-2 Rayleigh–Ritz variational approach to analysis the post-buckling behavior of cracked composite plates. This study was extended to the buckling and post-buckling of stiffened composite panels [27]. Xue et al. [28] investigated the free vibration of a stiffened plate with a side crack. The crack is through-the-thickness and starts from an arbitrary position on the edge of the flat plate. They found that the fundamental frequency decreased mildly with the crack length increase, then dropped drastically once the through-the-thickness crack broke the stiffener.

As an important component of the stiffened panel, the stiffener is expected to provide enhanced stiffness and stability to the structure with the extra advantage of lightweight. However, the effects of part-through cracks in stiffener on the vibration characteristic of stiffened plate remain unexplored. In previous research, there have been numerous studies focused on the modeling of cracks in beam structures. Swamidas et al. [29] presented a review on several main categories of the vibration models of the cracked beam. One of the earlier developed models was the local stiffness reduction method which introduced a short beam with a reduced bending stiffness to model the effect of crack [30]. Another model was the discrete spring model, which treated the cracked beam as two segments and connected both with a spring system at the crack location [31]. The stiffness of the spring was related to the depth of the crack and was determined by using the concepts of

fracture mechanics. The continuous cracked beam model has been developed to describe the crack effects properly, using either the stress or energy approach [32–35]. In addition, the local information of stress concentration at the crack tip, strain relief around the crack region, and continuous stiffness variation, have been considered in these models.

The Ritz method is one of the most successful methods to investigate dynamic, static, and buckling behavior of vibrating structures and to solve boundary value problems. Kumar [36] presented a comprehensive literature review on the application of the Ritz method to analyze vibration, static and buckling characteristics of beams [37–39], shells and plates based on different theories [40,41]. Most of the mentioned Rayleigh-Ritz solutions implemented the classical plate theory (CPT) [42–45]. Even though the CPT can be successfully applied to thin plates, it neglects both shear deformation and rotary inertia effects. The first-order shear deformation theory can eliminate the deficiency of the CPT and provide accurate results for the vibrations analysis of moderately thick or composite laminates [46–49]. Furthermore, compared to more sophisticated higher order plate theories, its low computational costs and simplicity make it an efficient method to solve such problems. On the other hand, the selection of the admissible functions in the Ritz method is essential to obtain accurate results. Pablo et al. [50] presented a literature review regarding the use of several sets of admissible functions in the Ritz method and compared the performance of the six different sets of admissible functions, namely characteristic functions (CF), modified characteristic functions (MCF), orthogonal polynomials (OP), non-orthogonal polynomials (NOP), product of trigonometric functions (PTF), static beam functions (SBF). The numerical behaviors of these functions are investigated to study the convergence of natural frequencies and corresponding mode shapes, the computational time, and the numerical stability in the free vibration analysis of a fully clamped rectangular plate. Pablo et al. [50] concluded that the MCF functions presented better numerical behavior when considering all the numerical features studied.

This paper aims to investigate the free vibration of a stiffened isotropic plate considering both cracked and intact stiffeners. The strain energy and kinetic energy of the flat plate and stiffeners are first expressed separately based on the first-order shear deformation theory, then combined through the compatibility conditions for the displacements of plate and stiffener. The continuous cracked beam model developed by energy formulations and fracture mechanics approach is extended to the cracked stiffener model considering the coupling of bending and longitudinal vibrations. The bending, torsional, and axial effects of the cracked and intact stiffeners on the stiffened plate are considered in this methodology. Natural frequencies and modes of the stiffened plate are obtained through the Ritz method with the modified characteristic functions. Parametric studies are conducted to determine the influence of crack parameters coupling with the position and the number of cracked stiffeners on the vibration characteristics of the stiffened plate. The accuracy of the presented solutions is verified through a convergence test and finite element results.

2 Theoretical formulations

2.1 Descriptions of the stiffened plate with crack

Consider a plate which is reinforced by a stiffener with a part-through crack and a intact stiffener at arbitrary location parallel to the x axis of coordinate (shown in Fig. 1). The global coordinate system (x,y,z) is located in the mid-plane of the plate in Cartesian coordinate system, while the local coordinate $(\bar{x},\bar{y},\bar{z})$ is set in the mid-plane of the intact stiffener at the distance of e_z from global coordinate. The geometry and dimension of a cracked stiffened plate are shown in Fig. 1.

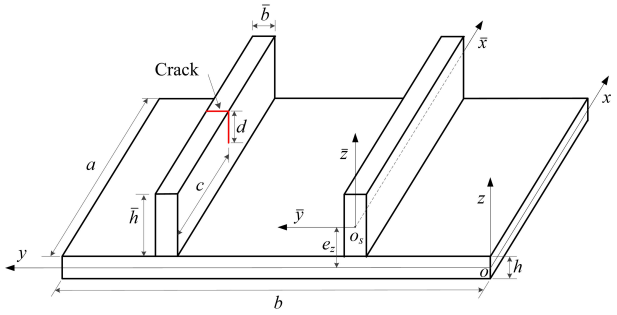

Figure 1: Geometry and dimensions of a stiffened plate with intact and cracked stiffeners.

2.2 Energy of plate

Based on the first-order shear deformation theory (FSDT), the displacements of an arbitrary point in the plate can be expressed as follows:

$$\left.\begin{aligned} u(x,y,z,t) &= u_0(x,y,t)+z\phi_x(x,y,t) \\ v(x,y,z,t) &= v_0(x,y,t)+z\phi_y(x,y,t) \\ w(x,y,z,t) &= w_0(x,y,t) \end{aligned}\right\}, \tag{2.1}$$

where u_0 and v_0 are the in-plane displacement components at the mid-plane points; w_0 is the mid-plane transverse displacement; φ_x and φ_y are the rotations in the y and x direction, respectively.

The strains associated with the displacements for the plate can be written as:

$$\left\{\begin{array}{c}\varepsilon_x\\ \varepsilon_y\\ \gamma_{xy}\end{array}\right\}=\left\{\begin{array}{c}\varepsilon_x^{(0)}\\ \varepsilon_y^{(0)}\\ \gamma_{xy}^{(0)}\end{array}\right\}+z\left\{\begin{array}{c}\varepsilon_x^{(1)}\\ \varepsilon_y^{(1)}\\ \gamma_{xy}^{(1)}\end{array}\right\}=\left\{\begin{array}{c}\dfrac{\partial u_0}{\partial x}\\ \dfrac{\partial v_0}{\partial y}\\ \dfrac{\partial u_0}{\partial y}+\dfrac{\partial v_0}{\partial x}\end{array}\right\}+z\left\{\begin{array}{c}\dfrac{\partial \phi_x}{\partial x}\\ \dfrac{\partial \phi_y}{\partial y}\\ \dfrac{\partial \phi_x}{\partial y}+\dfrac{\partial \phi_y}{\partial x}\end{array}\right\}, \tag{2.2a}$$

$$\left\{ \begin{array}{c} \gamma_{xz} \\ \gamma_{yz} \end{array} \right\} = \left\{ \begin{array}{c} \dfrac{\partial w_0}{\partial x} + \phi_x \\ \dfrac{\partial w_0}{\partial y} + \phi_y \end{array} \right\}. \tag{2.2b}$$

The strain energy (U_p) and the kinetic energy (T_p) of the plate based on FSDT are

$$\begin{aligned} U_p = \frac{1}{2} \iint_\Omega \Big[& N_x \varepsilon_x^{(0)} + M_x \varepsilon_x^{(1)} + N_y \varepsilon_y^{(0)} + M_y \varepsilon_y^{(1)} + N_{xy} \gamma_{xy}^{(0)} + M_{xy} \gamma_{xy}^{(1)} \\ & + Q_x \gamma_{xz} + Q_y \gamma_{yz} \Big] \, d\Omega, \end{aligned} \tag{2.3a}$$

$$T_p = \frac{\rho}{2} \int_{-h/2}^{h/2} \iint_\Omega \left(\dot{u}^2 + \dot{v}^2 + \dot{w}^2 \right) d\Omega dz, \tag{2.3b}$$

where Ω is in-plane surface area of the plate. The in-plane forces $(N_x, N_y, N_x y)$, moments $(M_x, M_y, M_x y)$ and transverse force (Q_x, Q_y) are expressed in terms of the strain resultants as follows:

$$N_x = \frac{Eh}{(1-v^2)} \left(\varepsilon_x^{(0)} + v \varepsilon_y^{(0)} \right), \quad N_y = \frac{Eh}{(1-v^2)} \left(\varepsilon_y^{(0)} + v \varepsilon_x^{(0)} \right), \quad N_{xy} = Gh \gamma_{xy}^{(0)}, \tag{2.4a}$$

$$M_x = D \left(\varepsilon_x^{(1)} + v \varepsilon_y^{(1)} \right), \quad M_y = D \left(\varepsilon_y^{(1)} + v \varepsilon_x^{(1)} \right), \quad M_{xy} = \frac{Gh^3}{12} \gamma_{xy}^{(1)}, \tag{2.4b}$$

$$Q_x = \kappa G h \gamma_{xz}, \quad Q_y = \kappa G h \gamma_{yz}, \tag{2.4c}$$

where $D = Eh^3/12(1-v)^2$ is the bending rigidity; E is the modulus of elasticity; v is Poisson's ratio; κ is the shear correction factor and set to $\pi^2/12$; G is the shear modulus $G = E/2(1+v)$. It should be noted that there is no coupling between the bending and the in-plane extension if there are no stiffeners on the isotropic plate.

2.3 Energy of intact and cracked stiffeners

The stiffener is modeled as a beam because the dimensions of cross-sectional are usually small in comparison to the length. $u_{s0}(o_s,t)$, $v_{s0}(o_s,t)$ and $w_{s0}(o_s,t)$ are the displacements of point o_s in $\bar{x}$, $\bar{y}$ and $\bar{z}$ axis directions, respectively, while $\varphi_{\bar{y}}$ is the rotation of the cross-section in the $(\bar{y},\bar{z})$ plane. Based on the compatibility condition for displacements between the plate and the stiffener, the displacement of point o_s can be expressed as

$$\left. \begin{array}{l} u\left(x=0, y=y_k, z=e_y, t\right) = u_0(0,y_k,t) + e_z \phi_x(0,y_k,t) = u_{s0}(o_s,t) \\ v\left(x=0, y=y_k, z=e_y, t\right) = v_0(0,y_k,t) + e_z \phi_y(0,y_k,t) = v_{s0}(o_s,t) \\ w\left(x=0, y=y_k, z=e_y, t\right) = w_0(0,y_k,t) = w_{s0}(o_s,t) \\ \phi_y(0,y_k,t) = \phi_{\bar{y}}(o_s,t) \end{array} \right\}, \tag{2.5}$$

where y_k is the location of stiffener in the y direction; e_z denotes the eccentricity from the mid-plane of the plate to the centroid of the individual stiffener.

The displacements at any point of the stiffener are expressed as

$$\left.\begin{aligned} u_s(\bar{x},\bar{y},\bar{z},t) &= u_0(x,y_k,t)+e_z\phi_x(x,y_k,t)+\bar{z}\phi_x(\bar{x},y_k,t) \\ v_s(\bar{x},\bar{y},\bar{z},t) &= v_0(x,y_k,t)+e_z\phi_y(x,y_k,t)+\bar{z}\phi_y(\bar{x},y_k,t) \\ w_s(\bar{x},\bar{y},\bar{z},t) &= w_0(x,y_k,t)-\bar{y}\phi_y(\bar{x},y_k,t) \end{aligned}\right\}, \tag{2.6}$$

where the displacements in the local coordinate system $(o_s\bar{x},\bar{y},\bar{z})$ can be transformed in the global coordinate system $(oxyz)$ according to the relationship of $x=\bar{x}$, $y=\bar{y}-y_k$ and $z=\bar{z}-e_z$.

The strains associated with the displacements for the stiffener at arbitrary location $\bar{y}=y_i$ parallel to the x axis are

$$\left.\begin{aligned} \varepsilon_{xs} &= \frac{\partial u_0}{\partial x}+e_z\frac{\partial \phi_x}{\partial x}+\bar{z}\frac{\partial \phi_x}{\partial x} \\ \gamma_{xzs} &= \frac{\partial w_0}{\partial x}+\phi_x-\bar{y}\frac{\partial \phi_y}{\partial x} \end{aligned}\right\}. \tag{2.7}$$

Thereafter, the strain energy $(U_s^{(i)})$ of the stiffener can be written as

$$\begin{aligned} U_s^{(i)} = \frac{1}{2}\int_0^a \Bigg\{ & E_s\bar{A}\left(\frac{\partial u_0}{\partial x}\right)^2+2E_s\bar{A}e_z\frac{\partial u_0}{\partial x}\frac{\partial \phi_x}{\partial x}+\left(E_s\bar{I}+E_s\bar{A}e_z^2\right)\frac{\partial \phi_x}{\partial x}\frac{\partial \phi_x}{\partial x} \\ & +\kappa G_s\bar{A}\left(\frac{\partial w_0}{\partial x}+\phi_x\right)\left(\frac{\partial w_0}{\partial x}+\phi_x\right)+\kappa G_s\bar{J}\frac{\partial \phi_y}{\partial x}\frac{\partial \phi_y}{\partial x}\Bigg\}dx\Bigg|_{\bar{y}=y_i}, \end{aligned} \tag{2.8}$$

where $A=\bar{b}\bar{h}$ is the area of stiffener cross section; $\bar{b}$ and $\bar{h}$ are the width and thickness of the stiffener, respectively; E_s and G_s are the elastic modulus and shear modulus, respectively; $\bar{I}$ is the second moment of area with respect to the stiffener's center of o_s; $\bar{J}$ is the saint-venant torsion constant of the stiffener

$$\bar{I}=\int_{\bar{A}}\bar{z}^2d\bar{A},\quad \bar{J}=\int_{\bar{A}}\bar{y}^2d\bar{A},\quad e_z=\frac{\bar{h}+h}{2}.$$

The first five terms in (2.8) are the strain energy of extensional, bending-extensional coupling, bending, shear and the torsional strain energy, respectively. The variable $\bar{y}$ in the strain energy $(U_s^{(i)})$ is equal to the position of the stiffener in the plate, i.e., $\bar{y}=y_i$.

The kinetic energy $(T_s^{(i)})$ of the stiffener is

$$T_s^{(i)}=\frac{\rho}{2}\int_{-h/2}^{h/2}\iint_{\bar{A}}\left(\dot{u_s}^2+\dot{v_s}^2+\dot{w_s}^2\right)d\bar{A}dz\Bigg|_{\bar{y}=y_i}. \tag{2.9}$$

Then, the strain energy and the kinetic energy of stiffener at arbitrary position of the plate can be obtained.

For the intact stiffeners, the strain energy $U_s^{(i)}$ and the kinetic energy $T_s^{(i)}$ can represent its contribution to the stiffened plate. When the structure has cracks, the stress concentration at the crack tip, strain relief around the crack region, and continuous stiffness variation will exist in the local area. The continuous cracked beam model [35], considering the stiffness loss at the crack location and the ineffectiveness of the material around the crack location, is extended to establish the model of the cracked stiffener. For a flexural plate coupled with the cracked stiffener, the effects of coupling between bending and longitudinal vibrations caused by the eccentricity of the stiffeners should be taken into account. Furthermore, the cracked stiffener positioned anywhere within the plate element should satisfy the compatibility conditions of displacements for stiffener and plate.

Based on the fracture mechanics and energy approach, the continuous equivalent bending stiffness of the cracked beam derived by Yang et al. [35] is given as

$$EI_c(x)=EI\left\{1+EIR(d,c)\Big/\left[1+\left(\frac{x-c}{k(d)d}\right)^2\right]\right\}^{-1}, \tag{2.10}$$

where EI is the bending stiffness of an intact beam; d and c are the depth and location of the crack, respectively; $EIR(d,c)$ and $k(d)$ are the parameters related to d and c, and have the forms below [26]

$$EIR(d,c)=3\pi[F(d)]^2 d\left\{k(d)\bar{h}\left[\arctan\left(\frac{l-c}{k(d)d}\right)+\arctan\left(\frac{c}{k(d)d}\right)\right]\right\}^{-1}, \tag{2.11a}$$

$$k(d)=3\pi[F(d)]^2(\bar{h}-d)^3 d\left\{\left[\bar{h}^3-(\bar{h}-d)^3\right]\bar{h}\right\}^{-1}, \tag{2.11b}$$

where $F(d)=1.12-1.4(d/\bar{h})+7.33(d/\bar{h})^2-13.8(d/\bar{h})^3+14(d/\bar{h})^4$.

Before obtaining the strain energy of the stiffener with a part-through crack, it is necessary to derive the extensional stiffness, bending stiffness, bending-extensional coupling stiffness, shear stiffness, and torsional stiffness of the cracked stiffener coupled to a flexural plate. Let $\bar{h}_{eq}(x)$ be the equivalent height of the cracked stiffener at any location x and has

$$\frac{EI}{EI_c(x)}=\frac{b\bar{h}^3/12}{b\bar{h}_{\rm eq}^3/12}=\frac{\bar{h}^3}{\bar{h}_{\rm eq}^3} \quad \text{and} \quad \bar{h}_{\rm eq}=\bar{h}^3\sqrt{\frac{EI_c(x)}{EI}}. \tag{2.12}$$

For the stiffness in the membrane strain, the bending strain, shear strain, and the torsional strain of the cracked stiffener, using (2.12), the following equation is presented

$$\left.\begin{aligned}
&\frac{E_S\bar{A}}{E_S\bar{A}_c(x)}=\frac{\bar{h}}{\bar{h}_{\rm eq}}=\sqrt[3]{\frac{EI}{EI_c(x)}}\\
&\frac{E_S\bar{I}}{E_S\bar{I}_c(x)}=\frac{\bar{h}^3}{\bar{h}_{\rm eq}^3}=\frac{EI}{EI_c(x)}\\
&\frac{\kappa G_S\bar{A}}{\kappa G_s\bar{A}_c(x)}=\frac{\bar{h}}{\bar{h}_{\rm eq}}=\sqrt[3]{\frac{EI}{EI_c(x)}}\\
&\frac{\kappa G_s\bar{J}}{\kappa G_S\bar{J}_c(x)}=\frac{\bar{h}}{\bar{h}_{\rm eq}}=\frac{EI}{EI_c(x)}
\end{aligned}\right\}. \tag{2.13}$$

Thereafter, substituting (2.10) into the above equation, one obtains the stiffness for the cracked stiffener as

$$\left.\begin{aligned} E_s\bar{A}_c(x) &= \frac{E_s\bar{A}}{\sqrt[3]{1+EIR(d,c)/[1+(\frac{x-c}{k(d)d})^2]}} \\ E_s\bar{I}_c(x) &= \frac{E_s\bar{I}}{1+EIR(d,c)/[1+(\frac{x-c}{k(d)d})^2]} \\ \kappa G_s\bar{A}_c(x) &= \frac{\kappa G_s\bar{A}}{\sqrt[3]{1+EIR(d,c)/[1+(\frac{x-c}{k(d)d})^2]}} \\ \kappa G_s\bar{J}_c(x) &= \frac{E_S\bar{I}}{1+EIR(d,c)/[1+(\frac{x-c}{k(d)d})^2]} \end{aligned}\right\}. \tag{2.14}$$

In addition, the thickness $\bar{h}$ of the cracked stiffener is replaced by the equivalent height $\bar{h}_{eq}$, and the eccentricity from the mid-plane of the plate to the centroid of the individual cracked stiffener $e_z c$ is obtained as

$$e_{zc} = (\bar{h}_{eq}(x)+h)/2. \tag{2.15}$$

The strain energy of cracked stiffener can be obtained and expressed as

$$\begin{aligned} U_s^{(i)} = \frac{1}{2}\int_0^a \Bigg\{ & E_s\bar{A}_c(x)\left(\frac{\partial u_0}{\partial x}\right)^2 + \left[E_s\bar{I}+E_s\bar{A}\left(\frac{\bar{h}_{\rm eq}(x)+h}{2}\right)^2\right]\frac{\partial\phi_x}{\partial x}\frac{\partial\phi_x}{\partial x} \\ & +2E_s\bar{A}_c(x)\frac{\bar{h}_{\rm eq}(x)+h}{2}\frac{\partial u_0}{\partial x}\frac{\partial\phi_x}{\partial x}+\kappa G_s\bar{A}_c(x)\left(\frac{\partial w_0}{\partial x}+\phi_x\right)\left(\frac{\partial w_0}{\partial x}+\phi_x\right) \\ & +\kappa G_s\bar{J}_c(x)\frac{\partial\phi_y}{\partial x}\frac{\partial\phi_y}{\partial x}\Bigg\}dx\Bigg|_{\bar{y}=y_i}. \end{aligned} \tag{2.16}$$

2.4 Ritz solution

The total strain energy of the stiffened plate with intact stiffeners and cracked stiffeners is given by

$$\begin{aligned} U_{\rm total} = & \frac{1}{2}\int_\Omega\Bigg[\frac{Eh}{(1-v^2)}\left(\frac{\partial u_0}{\partial x}+v\frac{\partial v_0}{\partial y}\right)\frac{\partial u_0}{\partial x}+D\left(\frac{\partial\phi_x}{\partial x}+v\frac{\partial\phi_y}{\partial y}\right)\frac{\partial\phi_x}{\partial x} \\ & +\frac{Eh}{(1-v^2)}\left(\frac{\partial v_0}{\partial y}+v\frac{\partial u_0}{\partial x}\right)\frac{\partial v_0}{\partial y}+D\left(\frac{\partial\phi_y}{\partial y}+v\frac{\partial\phi_x}{\partial x}\right)\frac{\partial\phi_y}{\partial y}+Gh\left(\frac{\partial u_0}{\partial y}+\frac{\partial v_0}{\partial x}\right)^2 \\ & +\frac{Gh^3}{12}\left(\frac{\partial\phi_x}{\partial y}+\frac{\partial\phi_y}{\partial x}\right)^2+\kappa Gh\left(\frac{\partial w}{\partial x}+\phi_x\right)^2+\kappa Gh\left(\frac{\partial w}{\partial y}+\phi_y\right)^2\Bigg]d\Omega \\ & +\sum_{i=1}^{Nt}\frac{1}{2}\int_0^a\Bigg[E_s\bar{A}\left(\frac{\partial u_0}{\partial x}+e_z\frac{\partial\phi_x}{\partial x}\right)^2+E_s\bar{I}\frac{\partial\phi_x}{\partial x}\frac{\partial\phi_x}{\partial x} \\ & +\kappa G_s\bar{A}\left(\frac{\partial w}{\partial x}+\phi_x\right)^2+\kappa G_s\bar{J}\frac{\partial\phi_y}{\partial x}\frac{\partial\phi_y}{\partial x}\Bigg]dx\Bigg|_{\bar{y}=y_i} \end{aligned}$$

$$+\sum_{j=1}^{Nc}\frac{1}{2}\int_0^a\left[E_s\overline{A_c}\left(\frac{\partial u_0}{\partial x}+e_z\frac{\partial\phi_x}{\partial x}\right)^2+E_s\bar{I}_c\frac{\partial\phi_x}{\partial x}\frac{\partial\phi_x}{\partial x}\right.$$
$$\left.+\kappa G_s\overline{A_c}\left(\frac{\partial}{\partial x}w+\phi_x\right)^2+\kappa G_s\bar{J}_c\left(\frac{\partial\phi_y}{\partial x}\right)^2\right]dx\Big|_{\bar{y}=y_j}, \tag{2.17}$$

where Nt and Nc are the numbers of the intact and cracked stiffeners, respectively; y_i and y_j denote the arbitrary locations of intact stiffener and cracked stiffener in the y direction of the plate, respectively, and $y_i\neq y_j$.

Considering the free vibration of a stiffened plate with harmonic motion of angular frequency ω, the kinetic energy becomes

$$\begin{aligned}T_{\text{total}}=&\frac{\omega^2\rho}{2}\int_\Omega\left[h\left(u_0^2+v_0^2+w^2\right)+\frac{h^3}{12}\left({\varphi_x}^2+\varphi_y^2\right)\right]d\Omega\\&+\sum_{i=1}^{Nt}\frac{\omega^2}{2}\rho\int_0^a\left\{\bar{A}\left[\left(e_z\phi_x+u_0\right)^2+\left(e_z\phi_y+v_0\right)^2+w^2\right]\right.\\&\left.+\left({\phi_x}^2+{\phi_y}^2\right)I_s+{\phi_y}^2I_k\right\}x\Big|_{\bar{y}=y_i}\\&+\sum_{j=1}^{Nc}\frac{\omega^2}{2}\rho\int_0^a\left\{\bar{A}\left[\left(e_z\phi_x+u_0\right)^2+\left(e_z\phi_y+v_0\right)^2+w^2\right]\right.\\&\left.+\left(\phi_x^2+\phi_y^2\right)I_s+{\phi_y}^2I_k\right\}dx\Big|_{\bar{y}=y_j},\end{aligned} \tag{2.18}$$

where $I_k=h_s\int_A\bar{y}^2\mathrm{d}A$.

In the Ritz method, the displacements of u_0, v_0, w, φ_x and φ_y can be expressed as

$$\left.\begin{aligned}u_0(x,y,t)&=\sum_{m=1}^{M}\sum_{n=1}^{N}A_{mn}^{(1)}X_m^{(1)}(x)Y_n^{(1)}(y)e^{i\omega t}\\v_0(x,y,t)&=\sum_{m=1}^{M}\sum_{n=1}^{N}A_{mn}^{(2)}X_m^{(2)}(x)Y_n^{(2)}(y)e^{i\omega t}\\w(x,y,t)&=\sum_{m=1}^{M}\sum_{n=1}^{N}A_{mn}^{(3)}X_m^{(3)}(x)Y_n^{(3)}(y)e^{i\omega t}\\\phi_x(x,y,t)&=\sum_{m=1}^{M}\sum_{n=1}^{N}A_{mn}^{(4)}X_m^{(4)}(x)Y_n^{(4)}(y)e^{i\omega t}\\\phi_y(x,y,t)&=\sum_{m=1}^{M}\sum_{n=1}^{N}A_{mn}^{(5)}X_m^{(5)}(x)Y_n^{(5)}(y)e^{i\omega t}\end{aligned}\right\}, \tag{2.19}$$

where $e^{i\omega t}$ is a time-harmonic function; $A_{mn}^{(g)}$, (g=1,2,3,4,5) are undetermined coefficients; $X_m^{(g)}(x)$ and $Y_n^{(g)}(y)$ are admissible functions of the displacements; Herein, M admissible

functions in the x direction and N functions in the y direction are used, giving $M\times N$ terms of admissible functions for each displacement.

Let $M=N$ and $A_{mn}^{(g)}=q_{M(m-1)+n}^{(g)}$, the undetermined coefficients $A_{mn}^{(g)}$, $(g=1,2,3,4,5)$ in (2.19) are assembled into vector $q^{(g)}=\{q_1^{(g)},q_2^{(g)},\cdots,q_{\bar{N}}^{(g)}\}^{\mathrm{T}}$ for convenience of presentation. $\bar{N}=M\times N$ is the total number of terms for admissible functions of each displacement. Similarly, the following notation is introduced

$$Q_k^{(g)}=Q_{\mathrm{M}(m-1)+n}^{(g)}=X_m^{(g)}(x)Y_n^{(g)}(y). \tag{2.20}$$

Thus, the functions of displacements in (2.19) can be expressed as

$$\sum_{m=1}^{M}\sum_{n=1}^{N}A_{mn}^{(g)}X_m^{(g)}(x)Y_n^{(g)}(y)=\sum_{k=1}^{\bar{N}}q_k^{(g)}Q_k^{(g)}(x,y). \tag{2.21}$$

The expression on the right side of (2.21) is more convenient for the following matrix operations.

The Ritz method is based on the minimization of the energy functional defined by the difference between the strain energy U_{total} and the kinetic energy T_{total}

$$\frac{\partial(U_{total}-T_{total})}{\partial q_k^{(g)}}=0,\quad g=1,2,3,4,5;\quad k=1,\cdots,\bar{N}. \tag{2.22}$$

The results in an eigenvalue problem related to natural frequencies and modes will be obtained by (2.22). Specifically, these equations are

$$\boldsymbol{Kq}=\omega^2\boldsymbol{Mq}, \tag{2.23}$$

where $\boldsymbol{q}=\{\boldsymbol{q^{(1)},q^{(2)},q^{(3)},q^{(4)},q^{(5)}}\}$; the stiffness K and mass matrices M are expressed in Appendix.

The crucial step to obtain a correct solution in Ritz method is to select an appropriate set of admissible functions which should be linearly independent, complete and satisfy the geometric boundary conditions of plate. Since the description of the crack parameters is based on the continuous equivalent bending stiffness and equivalent depth of the cracked beam, the proposed method is not limited by boundary conditions of displacements. Two typical boundary conditions are considered in this paper, i.e., simply supported plate with movable edges (SSSS) and clamped plate (CCCC). Thus, the boundary conditions of the displacements are

$$\text{SSSS}\qquad \left.\begin{array}{ll} v_0=w=\phi_y=0 & \text{at}\quad x=0,a \\ u_0=w=\phi_x=0 & \text{at}\quad y=0,b \end{array}\right\}, \tag{2.24a}$$

$$\text{CCCC}\qquad \left.\begin{array}{ll} u_0=v_0=w=\phi_x=\phi_y=0 & \text{at}\quad x=0,a \\ v_0=u_0=w=\phi_x=\phi_y=0 & \text{at}\quad y=0,b \end{array}\right\}. \tag{2.24b}$$

The MCF functions with good numerical stability are selected as the admissible functions of displacements. For transverse displacement w, $X_m^{(3)}(x)$ in (2.19) are defined as [43]

$$X_m^{(3)}(x)=C_{1m}\cos\left(\frac{r_m x}{a}\right)+C_{2m}\sin\left(\frac{r_m x}{a}\right)+C_{3m}e^{\frac{-r_m x}{a}}+C_{4m}e^{\frac{-r_m(a-x)}{a}}, \tag{2.25}$$

where the parameters r_m, C_{1m}, C_{2m}, C_{3m} and C_{4m} under the boundary condition of simply supported or clamped at both edges $(x=0,a)$ are given as follows

$$\text{SS} \qquad r_m=m\pi, \quad C_{1m}=C_{3m}=C_{4m}=0, \quad C_{2m}=\sqrt{2}, \tag{2.26a}$$

$$\text{CC} \quad \left.\begin{aligned} &\cos(r_m)-\frac{2e^{-r_m}}{1+e^{-2r_m}}=0, \quad C_{1m}=1, \quad C_{2m}=-\frac{1+(-1)^m e^{-r_m}}{1-(-1)^{m_e}e^{-r_m}} \\ &C_{3m}=-\frac{1}{1-(-1)^{m_e}e^{-r_m}}, \quad C_{4m}=-\frac{(-1)^m}{1-(-1)^m e^{-r_m}} \end{aligned}\right\}, \tag{2.26b}$$

where the parameters r_m of the CC boundary are the solutions of the nonlinear equation

$$\cos(r_m)-\frac{2\exp-2r_m}{1+\exp-2r_m}=0.$$

Similarly, the functions $Y_n^{(3)}(y)$ can be defined for the y direction by replacing the variable x for y, the width a for the length b, and m for n in (2.25).

For the SSSS with movable edges and CCCC with immovable edges, the admissible functions of in-plane displacements u_0 and v_0 in (2.19), which satisfy identically the boundary conditions, are expanded by using the following expressions

$$\text{SSSS} \quad \left.\begin{aligned} &X_m^{(1)}(x)Y_n^{(1)}(y)=\cos(m\pi x/a)\sin(n\pi y/b) \\ &X_m^{(2)}(x)Y_n^{(2)}(y)=\sin(m\pi x/a)\cos(n\pi y/b) \end{aligned}\right\}, \tag{2.27a}$$

$$\text{CCCC} \quad \left.\begin{aligned} &X_m^{(1)}(x)Y_n^{(1)}(y)=\sin(m\pi x/a)\sin(n\pi y/b) \\ &X_m^{(2)}(x)Y_n^{(2)}(y)=\sin(m\pi x/a)\sin(n\pi y/b) \end{aligned}\right\}. \tag{2.27b}$$

According to boundary conditions in (2.24a) and (2.24b), the admissible functions of rotations φ_x and φ_y of the SSSS and CCCC boundary conditions can be defined as

$$\text{SSSS} \quad \left.\begin{aligned} &X_m^{(4)}(x)Y_n^{(4)}(y)=\cos(m\pi x/a)\sin(n\pi y/b) \\ &X_m^{(5)}(x)Y_n^{(5)}(y)=\sin(m\pi x/a)\cos(n\pi y/b) \end{aligned}\right\}, \tag{2.28a}$$

$$\text{CCCC} \quad \left.\begin{aligned} &X_m^{(4)}(x)Y_n^{(4)}(y)=\sin(m\pi x/a)\sin(n\pi y/b) \\ &X_m^{(5)}(x)Y_n^{(5)}(y)=\sin(m\pi x/a)\sin(n\pi y/b) \end{aligned}\right\}. \tag{2.28b}$$

Thus, the admissible functions of the in-plane displacement, transverse displacement and rotations under different boundary conditions can be obtained.

3 Convergence study

The free vibration of a square plate reinforced by one stiffener is analyzed to verify the accuracy of the proposed approach. The boundary condition of the plate is SSSS. The location of the stiffener relative to the plate is $\bar{y}=0.5b$. The ratios of the stiffener dimensions to the plate thickness are $h_s/h=4$ and $b_s/h=1$, respectively. The crack in the stiffener is located at the location of $c=0.5b$ with a depth of $d=0.4\bar{h}$. The dimensions of the plate are $a\times b\times h=1\times 1\times 0.01$m, and the cross-section of the stiffener is $\bar{h}\times b_s=0.04\times 0.01$m. The material properties are $E=205.8$GPa, $\rho=7.83\times 10^3$kg/m^3 and $v=0.3$.

The variations of normalized equivalent stiffness (extensional stiffness and bending stiffness) and normalized equivalent eccentricity of the cracked stiffener (along its length) are shown in Fig. 2. The stiffness ratio denotes the ratio of the stiffness of the cracked stiffener to that of the intact stiffener.

The natural frequencies are determined by using (2.23) and are transferred to non-dimensional quantities by multiplying with $a^2\sqrt{\rho h/D}$. In Table 1, these frequencies were obtained by using 10, 12,13,14 and 15 MCF functions in both x and y-directions in (2.17). From Table 1, it can be observed that the frequencies of all orders tended to converge to the exact solutions with the increasing terms of MCF. The first three frequencies have converged to at least 3-digit accuracy when the numbers (M) of MCF functions are larger than 12. Since there are no such results published in the previous study, it will be verified by comparing with the shell finite element model via commercial software ABAQUS. The results of ABAQUS were obtained by using 88140 shell elements of type S4R. Table 1 shows that the finite element results are in good agreement with the solutions from the present approach with less computational effort. The relative difference of frequencies in

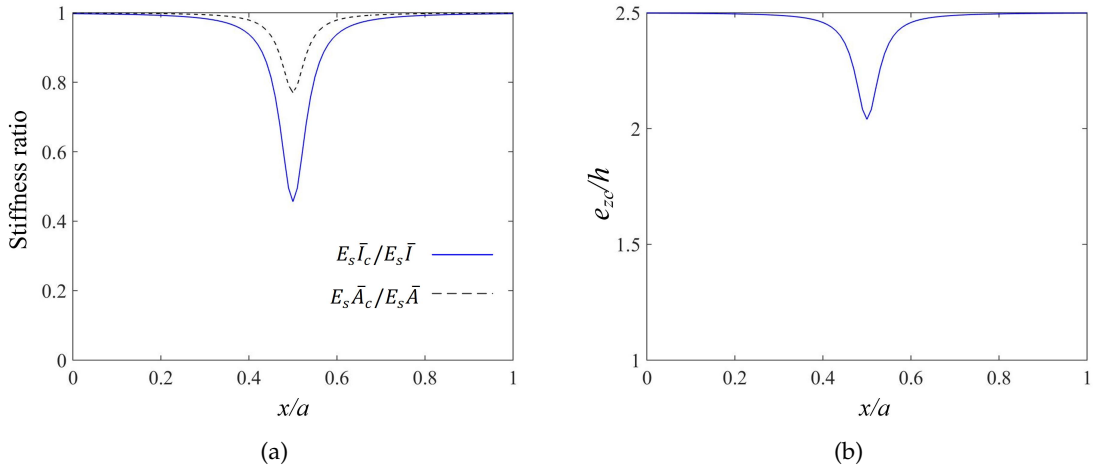

Figure 2: Variation of (a) normalized bending and extensional stiffness and (b) eccentricity of a stiffener with a crack.

Table 1: Convergence of non-dimensional frequency $\omega a^2\sqrt{\rho h/D}$ for an SSSS stiffened plate with a cracked stiffener.

Order of frequency	$M\times N$ 8×8	10×10	12×12	14×14	15×15	ABAQUS	Relative difference
		0	2	4			
1	28.75	28.7	28.67	28.64	28.62	28.42	0.70%
2	49.39	49.39	49.39	49.39	49.39	49.54	-0.30%
3	79.06	79.06	79.06	79.06	79.06	79.43	-0.47%
4	81.18	80.92	80.76	80.65	80.57	79.93	0.79%
5	97.34	97.33	97.32	97.31	97.3	97.05	0.26%

all cases is less than 0.79%, which indicates that the presented approach is accurate for the global responses. In addition, the most significant advantage is that no requirement of any modification should be applied to the model when the crack parameters change. However, the finite element method requires complicated work of remeshing. These results demonstrate the efficiency and accuracy of the present approach.

4 Modal analyses for the cracked stiffened plate

The effect of the cracks on the vibration characteristics of the stiffened plate depends not only on the crack parameters, but also on the size, number, and distribution of the stiffeners. In this section, the natural frequencies and corresponding modes of the stiffened plate are analyzed with various settings of geometric dimensions for stiffeners and cracks. The dimensions of the plate and the material properties for the stiffened plate are consistent with the previous section. $y_i^{(C)}$ and $y_i^{(T)}$ denote the location of the i-th cracked stiffener and intact stiffener, respectively. In the following analysis, the non-dimensional frequency parameters of the intact stiffened plate and the frequency ratio of the cracked stiffened plate are given. The frequency ratio denotes the ratio of the frequency of the cracked stiffened plate to that of the intact stiffened plate.

4.1 Cracked stiffener with different cross-sections

Two cross-sections of stiffeners are considered here (Section A and Section B). The geometric dimensions of Section A are $\bar{h}=4h$, $b_s=h$, and the Section B are $\bar{h}=5h$, $b_s=2h$. Table 2 presents the first five frequency ratios of the SSSS plate reinforced by one stiffener ($y_1^{(C)}=0.5b$) with a crack of various crack depths at different crack locations ($c/a=0.5$ and 0.75). The non-dimensional frequency parameters $\omega a^2\sqrt{\rho h/D}$ of intact stiffened plate are also given in brackets. It can be seen that the first-order, fourth-order and five-order natural frequencies decrease with an increasing depth of the crack. In addition, the crack has the most significant effect on the first-order frequency, while the second-order and third-order frequencies are insensitive to the crack and remain almost unchanged. It

Table 2: Frequency ratios of an SSSS stiffened plate with various crack depths and locations.

Section	c/b	$d/\bar{h}$	Order of frequency				
			1	2	3	4	5
A	0.5	0	1.0000	1.0000	1.0000	1.0000	1.0000
$\bar{h}/h=4$			(29.57)	(49.39)	(79.06)	(80.77)	(97.62)
$b_s/h=1$		0.1	0.9986	1	1	1	0.9998
		0.2	0.9936	1	1	0.9996	0.9993
		0.3	0.9838	1	1	0.9988	0.9984
		0.4	0.9679	1	1	0.9975	0.9967
		0.5	0.9412	1	0.9999	0.9946	0.9942
	0.75	0.1	0.9993	1	1	0.9995	0.9999
		0.2	0.997	1	1	0.9974	0.9997
		0.3	0.9919	1	1	0.9932	0.9992
		0.4	0.9831	1	1	0.9858	0.9984
		0.5	0.9669	1	1	0.973	0.997
B	0.5	0	10000	1.0000	1.0000	1.0000	1.0000
$\bar{h}/h=5$			(40.95)	(50.17)	(80.87)	(89.37)	(98.37)
$b_s/h=2$		0.1	0.9977	1	0.9999	1	0.9994
		0.2	0.9899	1	0.9998	0.9998	0.9975
		0.3	0.9757	1	0.9994	0.9993	0.994
		0.4	0.9516	0.9999	0.999	0.9985	0.9885
		0.5	0.9103	0.9998	0.9982	0.9966	0.9797
	0.75	0.1	0.999	1	1	0.9997	0.9998
		0.2	0.9951	0.9999	1	0.9986	0.9988
		0.3	0.9872	0.9998	0.9999	0.9963	0.9969
		0.4	0.9731	0.9996	0.9998	0.9923	0.9938
		0.5	0.9471	0.9992	0.9995	0.9847	0.9888

is also observed that the frequencies of the system with section B are more likely to be affected by the crack parameters than those of the system with section A, and a crack with depth $d/\bar{h}=0.5$ in section B can lead to a reduction in the first-order frequency by more than 8%. As the cross-section of the stiffener increases, the reinforcing effect of the stiffener on the stiffened plate increases, and the effect of the crack on the natural frequencies of the structure also becomes greater.

Table 3 shows the influence of various crack depths on the first five frequency ratios of the CCCC plate with one cracked stiffener ($y_1^{(C)}=0.5b$) at the crack locations of $c/a=0.5$. Unlike the situation of the SSSS stiffened plate, the first-order natural frequency of the CCCC stiffened plate with the sectional B remains almost unchanged due to the location of the stiffener is in coincidence with the nodal line of the mode.

Fig. 3 demonstrates the influence of crack location on the fundamental frequency of SSSS stiffened plates. Three crack depths ($d/\bar{h}=0.3$,0.4 and 0.5) and two kinds of cross-sections for the stiffener are taken into consideration. It should be noted that $c/a=0$ and $c/a=1$ mean the intact stiffened plate without crack. It is seen that the closer the crack

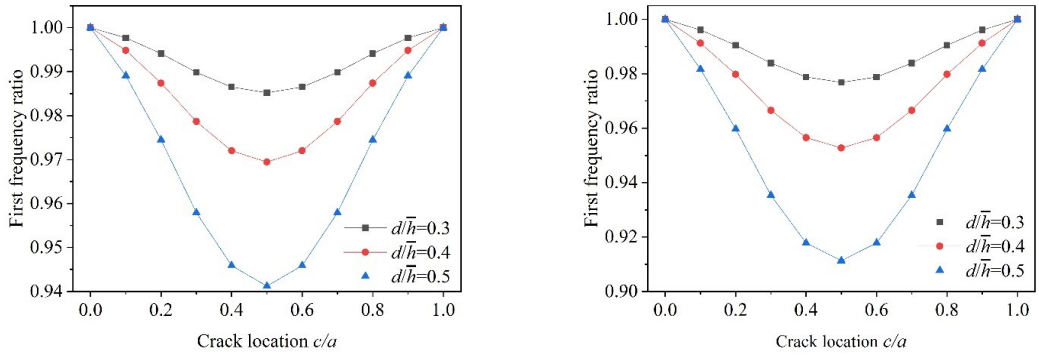

Figure 3: The fundamental frequency ratio of a SSSS stiffened plate with various crack depths and locations: (a) Section A; (a) Section B.

to the center $(x=0.5a$ or $c=0.5b)$ of the stiffener is, the lower the fundamental frequency will be, and the greatest reduction in the fundamental frequency occurs when the crack location (c/a) is 0.5. As both the structural geometry and boundary conditions of this stiffened plate are symmetrical, the curves of the fundamental frequency with various c/a are also symmetrical to the center line $(x=a/2)$. It is also observed that the difference of frequency difference between different crack depths becomes larger when the location is closer to the center.

Table 3: Frequency ratios of a CCCC stiffened plate with various crack depths.

Section	c/b	$d/\bar{h}$	Order of frequency				
			1	2	3	4	5
A	0.5	0	1	1	1	1	1
			(61.65)	(73.65)	(108.7)	(117)	(137.5)
$\bar{h}/h=4$		0.1	0.999	1	1	1	0.9997
$b_s/h=1$		0.2	0.9955	1	1	0.9997	0.9988
		0.3	0.9892	1	0.9999	0.9992	0.997
		0.4	0.979	1	0.9999	0.9982	0.9942
		0.5	0.9623	1	0.9998	0.9961	0.9898
B	0.5	0	1	1	1	1	1
			(74.58)	(78.99)	(79.06)	(111)	(123.6)
$\bar{h}/h=5$		0.1	1	0.999	0.9999	1	0.9991
$b_s/h=2$		0.2	1	0.9957	0.9997	0.9999	0.9961
		0.3	1	0.9898	0.9994	0.9996	0.9909
		0.4	0.9999	0.98	0.9988	0.999	0.9827
		0.5	0.9998	0.9637	0.998	0.9979	0.97

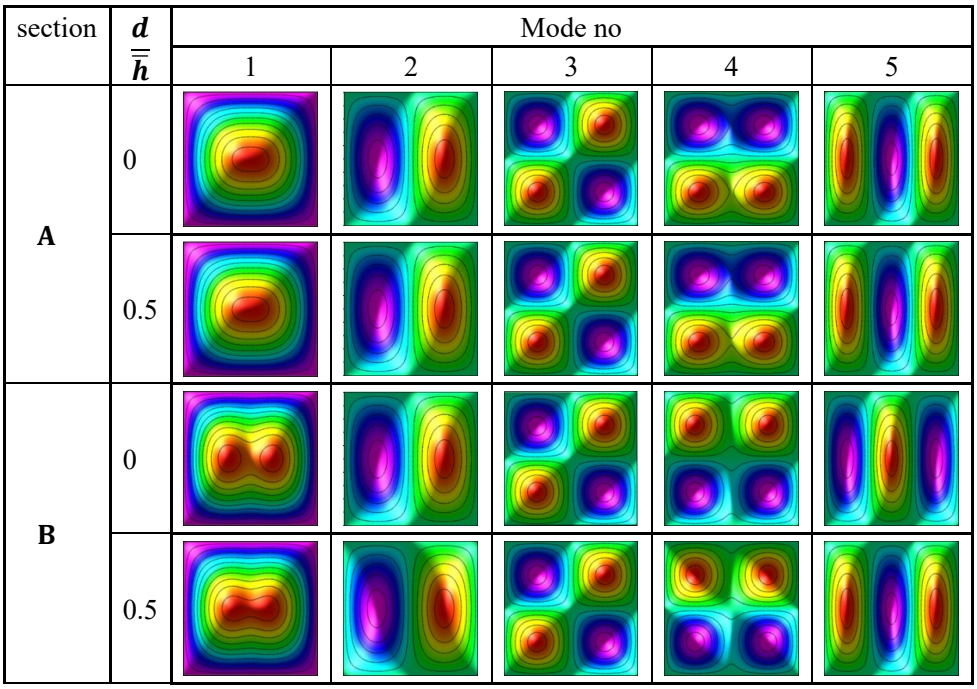

Figure 4: Modes of cracked SSSS stiffened plate with different stiffener sections $(c=0.5b)$.

The vibration modes of intact and cracked SSSS stiffened plate are presented in Fig. 6. Referring to the decrease of natural frequency for the stiffened plate with Section B in Table 1, the first-order mode which is changed obviously by the crack is different from the mode of the intact plate. The vibration modes of the stiffened plate under CCCC boundary conditions are shown in Fig. 5. Compared with the modes of the CCCC stiffened plate with Section A, the first two modes of the stiffened plate with Section B have been exchanged.

4.2 Stiffener with different numbers and crack depths

Next, four cases of settings of stiffener and crack, as shown in Fig. 5, are investigated. Case A: there are two stiffeners on the plate, one of which has a crack with varying crack depths. Case B: the stiffened plate reinforced by two cracked stiffeners with varying crack depths. Case C: there are three stiffeners on the plate, one of the stiffeners $(y_3^{(C)}=3b/4)$ has a crack with varying crack locations. Case D: there are three stiffeners on the plate, one of the stiffeners $(y_2^{(C)}=2b/4)$ has a crack with varying crack locations. The dimensions of the plate are $a\times b\times h=1\times 1\times 0.01$m, and the cross-section of the stiffener is $\bar{h}\times b_s=0.05\times 0.02$m. It should be noted that the boundary conditions of the stiffened

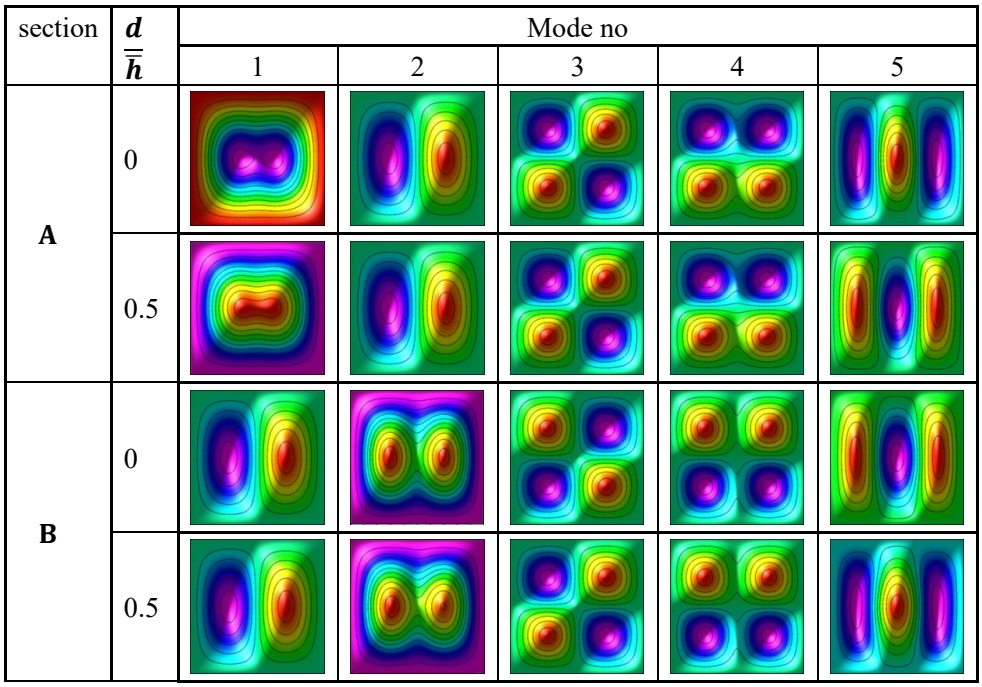

Figure 5: Modes of cracked CCCC stiffened plate with different stiffener sections $(c=0.5b)$.

plate here and in the following are both SSSS.

Table 4 presents the first five frequency ratios of stiffened plate, under Case A and B, reinforced by two stiffeners with various crack depths at location $c=0.5a$. For the stiffened plate with a cracked stiffener at $y_2^{(C)}=b/3$ or $y_1^{(C)}=2b/3$, the first five frequencies (except the third-order) are decreased with the increasing of crack depth. The crack on the stiffener has no effect on the third-order frequency due to the two stiffeners are located on the nodal line of the third-order mode. For the stiffened plate with a crack of $d=0.5a$, the first-order frequency is reduced by more than 6% compared with the intact plate. By contrast, two cracks with $d=0.5a$ in Case B lead to a reduction of the first-order frequency by more than 11%. As expected, the increased number of cracks can lead to an amount of reduction in the frequency of the plate. Fig. 8 depicts the first five-order modes of the intact and cracked stiffened plate (Cases A and B) with crack depth $d=0.5\bar{h}$. The first and third rows of the figure demonstrate the symmetric or anti-symmetric modes of the intact stiffened plate and Case B, respectively. For Case A, the crack in one stiffener causes the plate to be asymmetric along the y-axis, which also changes the symmetry of the modes, especially the first-order, fourth-order and fifth-order modes. Compared with the intact plate, the fourth and fifth-order modes of the cracked stiffened plate under Case A and B are exchanged because the fourth and fifth-order frequencies are very close, as shown in

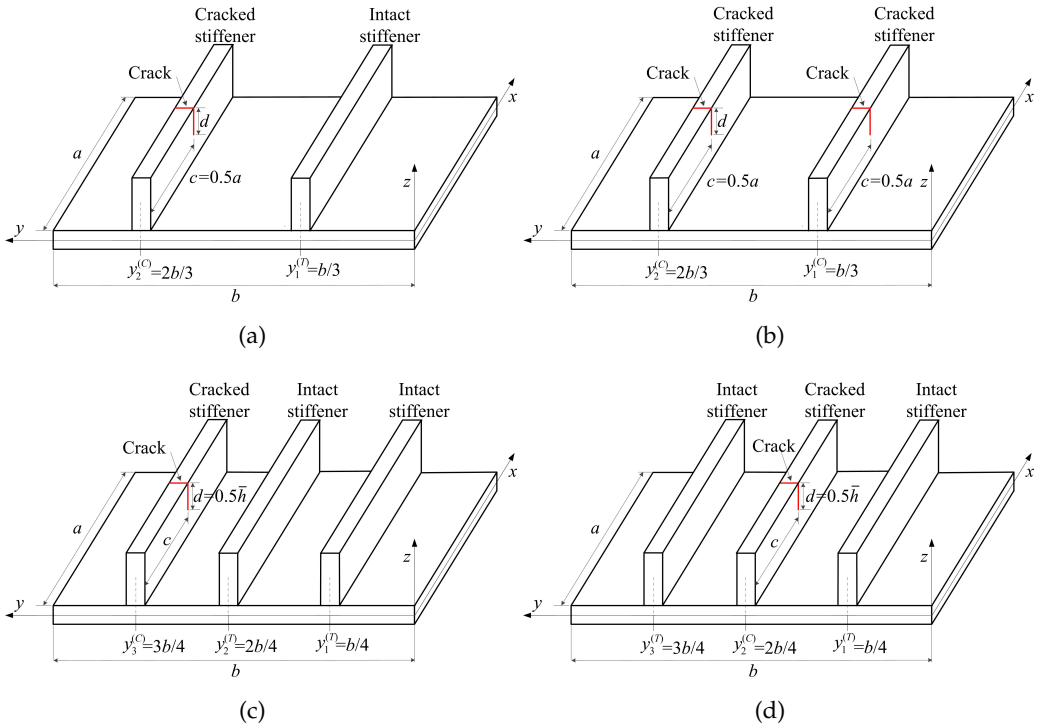

Figure 6: Four cases of cracked stiffened plates: (a) Case A with variable crack depths; (b) Case B with variable crack depths; (c) Case C with variable crack locations; (d) Case D with variable crack locations.

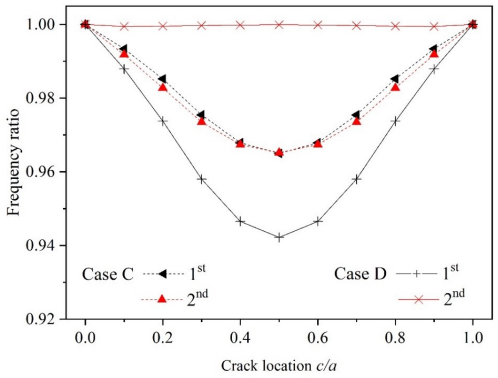

Figure 7: First two frequency ratios versus crack location under Case C and Case D.

Table 4.

Fig. 7 presents the first two frequency ratios versus crack location under Case C and Case D. It can be observed that the first two frequency ratios decrease with the crack

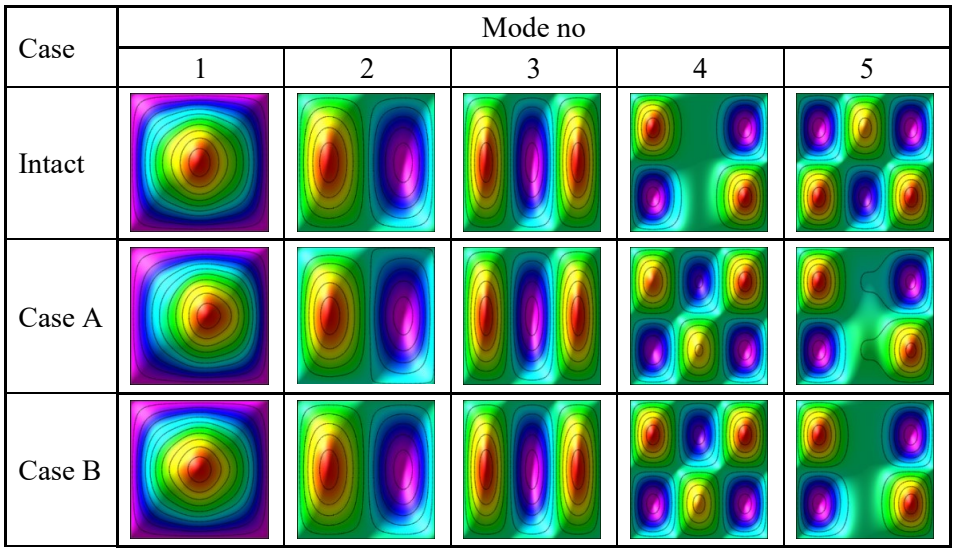

Figure 8: Modes of the stiffened plate under Cases A and B ($d/\bar{h}=0.5$).

placed closer to the center of the stiffener ($c=0.5a$). Comparing the first-order and second-order frequency ratios, it is found that the presence of a crack has a more significant effect on the fundamental (i.e., lowest) frequency than the second-order frequency. On the other hand, the location of the cracked stiffener can also affect the effect of the crack on the frequency. The phenomenon which the fundamental frequency of Case D ($y_2^{(C)}=2b/4$) is smaller than that of Case C ($y_3^{(C)}=b/4$), indicates that the closer the crack to the center of the plate ($x=a/2$, $y=b/2$) is, the smaller the fundamental frequency

Table 4: Frequency ratios of a CCCC stiffened plate with various crack depths.

		Order of frequency				
Case	$d/\bar{h}$	1	2	3	4	5
A	0	1	1	1	1	1
	0.1	0.9988	0.9993	1	1	1
	0.2	0.9941	0.9966	1	0.9998	0.9997
	0.3	0.9847	0.9916	1	0.9995	0.9993
	0.4	0.9681	0.984	1	0.9991	0.9983
	0.5	0.938	0.9729	0.9999	0.9984	0.9963
B	0.1	0.9976	0.9986	1	0.9999	0.9999
	0.2	0.9883	0.993	1	0.9996	0.9995
	0.3	0.9705	0.9825	1	0.9991	0.9985
	0.4	0.9403	0.9647	0.9999	0.9983	0.9967
	0.5	0.8895	0.935	0.9998	0.997	0.993

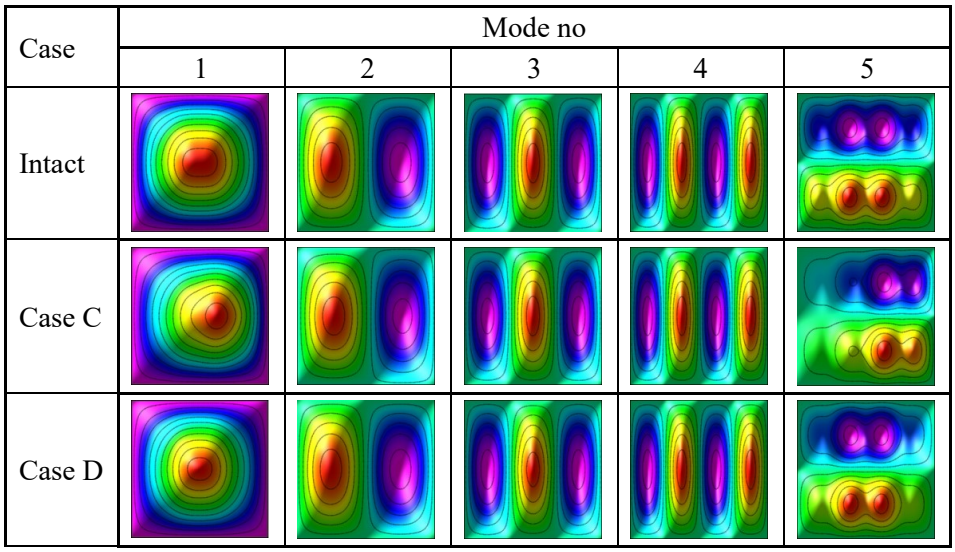

Figure 9: Modes cracked and intact stiffened plate under Case C and Case D $(c/a=0.5)$.

will be. Compared with the second-order frequency of Case C $(y_3^{(C)}=3b/4)$, that of Case C $(y_2^{(C)}=2b/4)$ is insensitive to the crack. This is because the location of the cracked stiffener at $y_2^{(C)}=2b/4$ coincides with the nodal line of second-order mode.

Fig. 9 depicts the first five-order modes of the intact and cracked stiffened plate (Case C and Case D) with crack location $c=0.5a$. As shown in the figure, no noticeable change in the modes is found due to the existence of a crack in Case D, while the crack in Case C can destroy the symmetry of the modes (especially the first-order and fifth-order modes).

5 Conclusions

The free vibration of a cracked stiffened plate is investigated through the Ritz method with the cracked stiffener model. The effect of crack parameters coupling with the position and number of the stiffeners on the natural frequencies and corresponding modes are investigated. The results from this paper are summarized as follows:

- The accuracy and efficiency of the proposed methodology have been substantiated through convergence studies of non-dimensional frequencies for simply supported stiffened plate with cracked stiffener. The convergent solutions of vibration frequencies show excellent agreement with those obtained by the commercial finite element package ABAQUS.

- The low-order frequency is sensitive to crack parameters and shows a significant reduction, except for the case that the cracked stiffener is consistent with the nodal line of the modes. For the crack location, the closer the crack is to the midpoint of the stiffener, the lower the natural frequency. A crack with a depth of $d=0.5\bar{h}$ on the stiffener will reduce the fundamental frequency of stiffened plate by almost 9%, although the dimensions of the crack are much smaller than the dimensions of the stiffened plate. These results suggest that even a small crack in the stiffener can significantly change the vibration characteristics of the stiffened plate.

- With the increase of the cross-section and number of cracked stiffeners, the reduction of the frequency caused by the crack also becomes more remarkable. Furthermore, the presence of cracks can destroy the symmetry of the stiffened plate and leads to an asymmetry in the modes.

Appendix

$$\mathbf{K}=\begin{bmatrix} \mathbf{K}^{u} & \mathbf{K}^{uv} & \mathbf{0} & \mathbf{K}^{u\phi_x} & \mathbf{0} \\ \mathbf{K}^{uv} & \mathbf{K}^{v} & \mathbf{0} & \mathbf{0} & \mathbf{0} \\ \mathbf{0} & \mathbf{0} & \mathbf{K}^{w} & \mathbf{K}^{w\phi_x} & \mathbf{K}^{w\phi_y} \\ \mathbf{K}^{\phi_x u} & \mathbf{0} & \mathbf{K}^{\phi_x w} & \mathbf{K}^{\phi_x} & \mathbf{K}^{\varphi_x\phi_y} \\ \mathbf{0} & \mathbf{0} & \mathbf{K}^{\phi_y w} & \mathbf{K}^{\phi_y\phi_x} & \mathbf{K}^{\phi_y} \end{bmatrix},$$

$$\mathbf{M}=\begin{bmatrix} \mathbf{M}^{u} & \mathbf{K}^{uv} & \mathbf{0} & \mathbf{M}^{u\phi_x} & \mathbf{0} \\ \mathbf{K}^{uv} & \mathbf{M}^{v} & \mathbf{0} & \mathbf{0} & \mathbf{M}^{v\phi_y} \\ \mathbf{0} & \mathbf{0} & \mathbf{M}^{w} & \mathbf{0} & \mathbf{0} \\ \mathbf{M}^{\phi_x u} & \mathbf{0} & \mathbf{0} & \mathbf{M}^{\phi_x} & \mathbf{0} \\ \mathbf{0} & \mathbf{M}^{\phi_y v} & \mathbf{0} & \mathbf{0} & \mathbf{M}^{\phi_y} \end{bmatrix},$$

$$\mathbf{M}=\mathbf{diag}[\mathbf{M}^{u}\mathbf{M}^{u}\mathbf{M}^{w}\mathbf{M}^{\varphi_x}\mathbf{M}^{\varphi_y}],$$

where the components in the forgoing block matrices are

$$K^{u}_{kl}=\sum_{i=1}^{Nt}\int_S\left[E_s\bar{A}Q^{(1)}_{k,x}Q^{(1)}_{l,x}\right]dx\bigg|_{\bar{y}=y_i}+\sum_{j=1}^{Nc}\int_S\left[E_s\bar{A}_cQ^{(1)}_{k,x}Q^{(1)}_{l,x}\right]dx\bigg|_{\bar{y}=y_j}$$
$$+\iint_\Omega\left(\frac{Eh}{1-v^2}Q^{(1)}_{k,x}Q^{(1)}_{l,x}+\frac{Eh}{2(1+v)}Q^{(1)}_{k,y}Q^{(1)}_{l,y}\right)dxdy,$$
$$K^{uv}_{kl}=K^{vu}_{kl}=\iint_\Omega\left(\frac{Ehv}{1-v^2}Q^{(1)}_{k,x}Q^{(2)}_{l,y}+\frac{Eh}{2(1+v)}Q^{(1)}_{k,y}Q^{(2)}_{l,x}\right)dxdy,$$
$$K^{v}_{kl}=\iint_\Omega\left(\frac{Eh}{1-v^2}Q^{(2)}_{k,y}Q^{(2)}_{l,y}+\frac{Eh}{2(1+v)}Q^{(2)}_{k,x}Q^{(2)}_{l,x}\right)dxdy,$$

$$K_{kl}^{u\phi_x}=K_{kl}^{\phi_x u}=\sum_{i=1}^{Nt}\int_S\left[E_s\bar{A}e_z Q_{k,x}^{(1)}Q_{l,x}^{(4)}\right]dx\Bigg|_{\bar{y}=y_i}+\sum_{j=1}^{Nc}\int_S\left[E_s\bar{A}_c e_z Q_{k,x}^{(1)}Q_{l,x}^{(4)}\right]dx\Bigg|_{\bar{y}=y_j},$$

$$K_{kl}^{\phi_x u}=\sum_{j=1}^{Nc}\int_l\left[E_s\overline{A_c}e_z Q_{k,x}^{(4)}Q_{l,x}^{(1)}\right]dx\Bigg|_{\bar{y}=y_j},$$

$$K_{kl}^{w}=\sum_{i=1}^{Nt}\int_S\left[\kappa G_s\bar{A}Q_{k,x}^{(4)}Q_{l,x}^{(4)}\right]dx\Bigg|_{\bar{y}=y_i}+\sum_{j=1}^{Nc}\int_S\left[\kappa G_s\overline{A_c}Q_{k,x}^{(4)}Q_{l,x}^{(4)}\right]dx\Bigg|_{\bar{y}=y_j}$$
$$+\iint_\Omega\kappa Gh\left(Q_{k,x}^{(3)}Q_{l,x}^{(3)}+Q_{k,y}^{(3)}Q_{l,y}^{(3)}\right)dxdy,$$

$$K_{kl}^{w\phi_x}=K_{lk}^{\phi_x w}=\iint_\Omega\kappa GhQ_{k,x}^{(3)}Q_{l,x}^{(4)}dxdy+\sum_{i=1}^{Nt}\int_S\left[\kappa G_s\bar{A}Q_{k,x}^{(4)}Q_{l}^{(4)}\right]dx\Bigg|_{\bar{y}=y_i}$$
$$+\sum_{j=1}^{Nc}\int_S\left[\kappa G_s\bar{A}_c Q_{m,x}^{(4)}Q_{n}^{(4)}\right]dx\Bigg|_{\bar{y}=y_j},$$

$$K_{kl}^{w\phi_y}=K_{lk}^{\phi_y w}=\iint_\Omega\kappa GhQ_{k,y}^{(3)}Q_{l,y}^{(5)}dxdy,$$

$$K_{kl}^{\phi_x}=\sum_{i=1}^{Nt}\int_S\left[E_S\bar{A}e_Z^2Q_{k,x}^{(4)}Q_{l,x}^{(4)}+E_S\bar{I}Q_{k,x}^{(4)}Q_{l,x}^{(4)}+\kappa G_s\bar{A}Q_k^{(4)}Q_l^{(4)}\right]dx\Bigg|_{\bar{y}=y_i}$$
$$+\sum_{j=1}^{Nc}\int_S\left[E_s\bar{A}_c e_z^2Q_{k,x}^{(4)}Q_{l,x}^{(4)}+E_s\bar{I}_cQ_{k,x}^{(4)}Q_{l,x}^{(4)}+\kappa G_s\bar{A}_cQ_k^{(4)}Q_l^{(4)}\right]dx\Bigg|_{\bar{y}=y_j}$$
$$+\iint_\Omega\left\{\frac{D}{2}\left[2Q_{k,x}^{(4)}Q_{l,x}^{(4)}+(1-v)Q_{k,y}^{(4)}Q_{l,y}^{(4)}\right]+\kappa GhQ_k^{(4)}Q_l^{(4)}\right\}dxdy,$$

$$K_{kl}^{\phi_y}=\sum_{i=1}^{Nt}\int_S\left[\kappa G_s\bar{J}Q_{k,x}^{(5)}Q_{l,x}^{(5)}\right]dx\Bigg|_{\bar{y}=y_i}+\sum_{j=1}^{Nc}\int_S\left[\kappa G_s\bar{J}_cQ_{m,x}^{(5)}Q_{n,x}^{(5)}\right]dx\Bigg|_{\bar{y}=y_j}$$
$$+\iint_\Omega\left\{\frac{D}{2}\left[Q_{k,y}^{(5)}Q_{l,y}^{(5)}+(1-v)Q_{k,x}^{(5)}Q_{l,x}^{(5)}\right]+\kappa GhQ_k^{(5)}Q_l^{(5)}\right\}dxdy,$$

$$K_{kl}^{\phi_x\phi_y}=K_{kl}^{\phi_y\phi_x}=\iint_A\frac{D}{2}(1+v)Q_{k,y}^{(4)}Q_{l,x}^{(5)}dxdy,$$

$$M_{kl}^{u}=\sum_{i=1}^{Nt}\rho\int_S\bar{A}Q_k^{(1)}Q_l^{(1)}dx\Bigg|_{\bar{y}=y_i}+\sum_{j=1}^{Nc}\frac{\omega^2}{2}\rho\int_S\bar{A}Q_k^{(1)}Q_l^{(1)}dx\Bigg|_{\bar{y}=y_j},$$

$$M_{kl}^{v}=\sum_{i=1}^{Nt}\rho\int_S\bar{A}Q_k^{(2)}Q_l^{(2)}dx\Bigg|_{\bar{y}=y_i}+\sum_{j=1}^{Nc}\frac{\omega^2}{2}\rho\int_S\bar{A}Q_k^{(2)}Q_l^{(2)}dx\Bigg|_{\bar{y}=y_j},$$

$$M_{kl}^{u\phi_x}=M_{kl}^{\phi_x u}=\sum_{i=1}^{Nt}\int_S\left[\bar{A}e_zQ_{k,x}^{(1)}Q_{l,x}^{(4)}\right]dx\Bigg|_{\bar{y}=y_i}+\sum_{j=1}^{Nc}\int_S\left[\bar{A}e_zQ_{k,x}^{(1)}Q_{l,x}^{(4)}\right]dx\Bigg|_{\bar{y}=y_j},$$

$$M_{kl}^{v\phi_y}=M_{kl}^{\phi_y^v}=\sum_{i=1}^{Nt}\int_S\left[\bar{A}e_z Q_{k,x}^{(2)}Q_{l,x}^{(5)}\right]dx\Big|_{\bar{y}=y_i}+\sum_{j=1}^{Nc}\int_S\left[\bar{A}e_z Q_{k,x}^{(2)}Q_{l,x}^{(5)}\right]dx\Big|_{\bar{y}=y_j},$$

$$M_{kl}^{w}=\sum_{i=1}^{Nt}\rho\int_S\bar{A}Q_k^{(3)}Q_l^{(3)}dx\Big|_{\bar{y}=y_i}+\sum_{j=1}^{Nc}\rho\int_S\bar{A}Q_k^{(3)}Q_l^{(3)}dx\Big|_{\bar{y}=y_j}+\iint_\Omega\rho hQ_k^{(3)}Q_l^{(3)}dxdy,$$

$$\begin{aligned}M_{kl}^{\phi_x}=&\sum_{i=1}^{Nt}\rho\int_S\bar{A}e_z^2Q_k^{(4)}Q_l^{(4)}dx\Big|_{\bar{y}=y_i}+\sum_{i=1}^{Nt}\rho\int_S^{-1}I_sQ_k^{(4)}Q_l^{(4)}dx\Big|_{\bar{y}=y_i}+\sum_{j=1}^{Nc}\rho\int_S\bar{A}e_z^2Q_k^{(4)}Q_l^{(4)}dx\Big|_{\bar{y}=y_j}\\&+\sum_{j=1}^{Nc}\rho\int_SI_sQ_k^{(4)}Q_l^{(4)}dx\Big|_{\bar{y}=y_j}+\iint_\Omega\frac{1}{12}\rho h^3Q_k^{(4)}Q_l^{(4)}dxdy,\end{aligned}$$

$$\begin{aligned}M_{kl}^{\phi_y}=&\sum_{i=1}^{Nt}\rho\int_S\bar{A}e_z^2Q_k^{(5)}Q_l^{(5)}dx\Big|_{\bar{y}=y_i}+\sum_{i=1}^{Nt}\rho\int_S(I_s+I_k)Q_k^{(5)}Q_l^{(5)}dx\Big|_{\bar{y}=y_i}+\sum_{j=1}^{Nc}\rho\int_S\bar{A}e_z^2Q_k^{(5)}Q_l^{(5)}dx\Big|_{\bar{y}=y_j}\\&+\sum_{j=1}^{Nc}\rho\int_S(I_s+I_k)Q_k^{(5)}Q_l^{(5)}dx\Big|_{\bar{y}=y_j}+\iint_\Omega\frac{1}{12}\rho h^3Q_k^{(4)}Q_l^{(4)}dxdy.\end{aligned}$$

Acknowledgements

This paper is supported by the national natural science foundation of China, project Nos. 11972053 and 11772013. We really appreciate the assistance of the committee of the national natural science foundation of China.

References

[1] A. MUKHERJEE, AND M. MUKHOPADHYAY, *Review of dynamic behavior of stiffened plates,* Shock Vib. Dig., 18 (1986), pp. 3–8.

[2] O. BEDAIR, *Analysis and limit state design of stiffened plates and shells: A world view,* Appl. Mech. Rev., 62 (2009), pp. 1–16.

[3] K. M. LIEW, Y. XIANG, S. KITIPORNCHAI, AND J. L. MEEK, *Formulation of Mindlin-Engesser model for stiffened plate vibration*, Comput. Methods Appl. Mech. Eng., 120 (1995), pp. 339–353.

[4] B. H. S. OLIVEIRA, E. LUCENA NETO, AND F. A. C. MONTEIRO, *An accurate Ritz approach for analysis of cracked stiffened plates,* Appl. Math. Model., 73 (2019), pp. 598–614.

[5] A. BERRY, AND C. LOCQUETEAU, *Vibration and sound radiation of fluid-loaded stiffened plates with consideration of in-plane deformation,* J. Acoust. Soc. Am., 100 (1996), pp. 312–319.

[6] L. SINHA, S. S. MISHRA, A. N. NAYAK, AND S. K. SAHU, *Free vibration characteristics of laminated composite stiffened plates: Experimental and numerical investigation,* Compos. Struct., 233 (2020).

[7] L. PRATICÒ, J. GALOS, E. CESTINO, G. FRULLA, AND P. MARZOCCA, *Experimental and numerical vibration analysis of plates with curvilinear sub-stiffeners,* Eng. Struct., 209 (2020), p. 109956.

[8] I. E. HARIK, AND M. GUO, *Finite element analysis of eccentrically stiffened plates in free vibration,* Comput. Struct., 49 (1993), pp. 1007–1015.
[9] D. LI, AND Y. LIU, *Three-dimensional semi-analytical model for the static response and sensitivity analysis of the composite stiffened laminated plate with interfacial imperfections,* Compos. Struct., 94 (2012), pp. 1943–1958.
[10] S. N. PATEL, P. K. DATTA, AND A. H. SHEIKH, *Parametric study on the dynamic instability behavior of laminated composite stiffened plate,* J. Eng. Mech., 135 (2009), pp. 1331–1341.
[11] M. BOSCOLO, AND J. R. BANERJEE, *Layer-wise dynamic stiffness solution for free vibration analysis of laminated composite plates,* J. Sound Vib., 333 (2014), pp. 200–227.
[12] E. DAMNJANOVIĆ, M. MARJANOVIĆ, AND M. NEFOVSKA-DANILOVIĆ, *Free vibration analysis of stiffened and cracked laminated composite plate assemblies using shear-deformable dynamic stiffness elements,* Compos. Struct., 180 (2017), pp. 723–740.
[13] M. NEFOVSKA-DANILOVIC, N. KOLAREVIC, M. MARJANOVIĆ, AND M. PETRONIJEVIC, *Shear deformable dynamic stiffness elements for a free vibration analysis of composite plate assemblies–Part I: Theory,* Compos. Struct., 159 (2017), pp. 728–744.
[14] E. DAMNJANOVIĆ, M. NEFOVSKA-DANILOVIĆ, M. PETRONIJEVIĆ, AND M. MARJANOVIĆ, *Application of the dynamic stiffness method in the vibration analysis of stiffened composite plates,* Procedia Eng., 199 (2017), pp. 224–229.
[15] H. ZENG, AND C. W. BERT, *A differential quadrature analysis of vibration for rectangular stiffened plates,* J. Sound Vib., 241 (2001), pp. 247–252.
[16] L. X. PENG, K. M. LIEW, AND S. KITIPORNCHAI, *Buckling and free vibration analyses of stiffened plates using the FSDT mesh-free method,* J. Sound Vib., 289 (2006), pp. 421–449.
[17] A. Y. TAMIJANI, AND R. K. KAPANIA, *Vibration analysis of curvilinearly-stiffened functionally graded plate using element free galerkin method,* Mech. Adv. Mater. Struct., 19 (2012), pp. 100–108.
[18] J. XUE, Y. WANG, AND L. CHEN, *Nonlinear vibration of cracked rectangular Mindlin plate with in-plane preload,* J. Sound Vib., 481 (2020), p. 115437.
[19] A. MILAZZO, AND V. OLIVERI, *Investigation of buckling characteristics of cracked variable stiffness composite plates by an eXtended Ritz approach,* Thin-Walled Struct., 163 (2021), p. 107750.
[20] J. XUE, Y. WANG, L. CHEN, *Buckling and free vibration of a side-cracked Mindlin plate under axial in-plane load,* Arch. Appl. Mech., 90 (2020), pp. 1811–1827.
[21] Y. SONG, K. XUE, AND Q. LI, *A solution method for free vibration of intact and cracked polygonal thin plates using the Ritz method and Jacobi polynomials,* J. Sound Vib., 519 (2022), p. 116578.
[22] Y. WU, Z. XIAO, D. LI, AND J. XU, *On numerical static analysis of stiffened laminated composite plates with delaminations, cracks, or debonding of a piezoelectric patch,* Mech. Adv. Mater. Struct., 0 (2020), pp. 1–15.
[23] D. LI, *Layerwise theories of laminated composite structures and their applications: a review,* Arch. Comput. Methods Eng., 28 (2021), pp. 577–600.
[24] J. X. XU, Z. G. XIAO, Y. G. WU, AND D. H. LI, *Extended layerwise method for laminated piezoelectric and composite plates with delaminations, cracks or debonding of a piezoelectric patch,* Compos. Struct., 234 (2020).
[25] T. D. DANG, AND R. K. KAPANIA, *Ritz approach for buckling prediction of cracked-stiffened structures,* J. Aircr., 50 (2013), pp. 965–974.
[26] A. MILAZZO, AND V. OLIVERI, *Post-buckling analysis of cracked multilayered composite plates by pb-2 Rayleigh-Ritz method,* Compos. Struct., 132 (2015), pp. 75–86.
[27] A. MILAZZO, AND V. OLIVERI, *Buckling and postbuckling of stiffened composite panels with cracks and delaminations by ritz approach,* AIAA J., 55 (2017), pp. 965–980.

[28] J. XUE, AND Y. WANG, *Free vibration analysis of a flat stiffened plate with side crack through the Ritz method,* Arch. Appl. Mech., 89 (2019), pp. 2089–2102.
[29] A. S. J. SWAMIDAS, X. YANG, AND R. SESHADRI, *Timoshenko and Euler formulations,* J. Eng. Mech., 130 (2004), pp. 1297–1308.
[30] W. T. THOMSON, *Vibration of slender bars with discontinuities in stiffness,* J. Appl. Mech. Asme., 16 (1949), pp. 203–208.
[31] H. OKAMURA, K. WATANABE, AND T. TAKANO, *Applications of the compliance concept in fracture mechanics,* ASTM Spec. Tech. Publ., 536 (1972), pp. 423–438.
[32] S. CHRISTIDES, AND A. D. S. BARR, *One-dimensional theory of cracked Bernoulli-Euler beams,* Int. J. Mech. Sci., 26 (1984), pp. 639–648.
[33] M. H. H. SHEN, AND C. PIERRE, *Free Vibrations of Beams With a Single-Edge Crack,* J. Sound Vib., 170 (1994), pp. 237–259.
[34] T. G. CHONDROS, AND A. D. DIMAROGONAS, *Vibration of a cracked cantilever beam,* J. Vib. Acoust. Trans. ASME, 120 (1998), pp. 742–746.
[35] X. F. YANG, A. S. J. SWAMIDAS, AND R. SESHADRI, *Crack identification in vibrating beams using the energy method,* J. Sound Vib., 244 (2001), pp. 339–357.
[36] Y. KUMAR, *The Rayleigh–Ritz method for linear dynamic, static and buckling behavior of beams, shells and plates: A literature review,* J. Vib. Control., 24 (2018), pp. 1205–1227.
[37] J. YANG, G. SUN, AND J. YANG, *Bifurcation and chaos of functionally graded carbon nanotube reinforced composite beam with piezoelectric layer,* Adv. Appl. Math. Mech., 13 (2021), pp. 569–589.
[38] Ş.D. ALBAS, H. ERSOY, B. AKGÖZ, AND Ö. CIVALEK, *Dynamic analysis of a fiber-reinforced composite beam under a moving load by the ritz method,* Mathematics, 9 (2021).
[39] Ö. CIVALEK, S. DASTJERDI, Ş.D. AKBAŞ, AND B. AKGÖZ, *Vibration analysis of carbon nanotube-reinforced composite microbeams,* Math. Methods Appl. Sci., (2021), pp. 1–17.
[40] A. E. ABOUELREGAL, AND A. M. ZENKOUR, *On the generalized thermoelasticity problem for an infinite fibre-reinforced thick plate under initial stress,* Adv. Appl. Math. Mech., 6 (2014), pp. 783–796.
[41] S. DASTJERDI, B. AKGÖZ, AND Ö. CIVALEK, *On the effect of viscoelasticity on behavior of gyroscopes,* Int. J. Eng. Sci., 149 (2020).
[42] D. G. STAMATELOS, G. N. LABEAS, AND K. I. TSERPES, *Analytical calculation of local buckling and post-buckling behavior of isotropic and orthotropic stiffened panels,* Thin-Walled Struct., 49 (2011), pp. 422–430.
[43] L. BRUBAK, AND J. HELLESLAND, *Semi-analytical postbuckling analysis of stiffened imperfect plates with a free or stiffened edge,* Comput. Struct., 89 (2011), pp. 1574–1585.
[44] R. VESCOVINI, AND C. BISAGNI, *Two-step procedure for fast post-buckling analysis of composite stiffened panels,* Comput. Struct., 128 (2013), pp. 38–47.
[45] H. ZHENG, AND Z. WEI, *Vibroacoustic analysis of stiffened plates with nonuniform boundary conditions,* Int. J. Appl. Mech., 5 (2013).
[46] K. M. LIEW, *Solving the vibation of thick symmetric laminates by Reissner/Mindlin plate theory and the p-Ritz method,* J. Sound Vib., 198 (1996), pp. 343–360.
[47] Y. K. CHEUNG, AND D. ZHOU, *Vibrations of moderately thick rectangular plates in terms of a set of static Timoshenko beam functions,* Comput. Struct., 78 (2000), pp. 757–768.
[48] D. ZHOU, *Vibrations of Mindlin rectangular plates with elastically restrained edges using static Timoshenko beam functions with the Rayleigh-Ritz method,* Int. J. Solids Struct., 38 (2001), pp. 5565–5580.
[49] S. A. EFTEKHARI, AND A. A. JAFARI, *A simple and accurate Ritz formulation for free vibration of*

thick rectangular and skew plates with general boundary conditions, Acta Mech., 224 (2013), pp. 193–209.

[50] P. MORENO-GARCÍA, J. V. A. DOS SANTOS, AND H. LOPES, *A review and study on ritz method admissible functions with emphasis on buckling and free vibration of isotropic and anisotropic beams and plates,* Arch. Comput. Methods Eng., 25 (2018), pp. 785–815.

[51] J. R. GARTNER, AND N. OLGAC, *Improved numerical computation of uniform beam characteristic values and characteristic functions,* J. Sound Vib., 84 (1982), pp. 481–489.